Materials Horizons

REVIEW

View Article Online
View Journal

Cite this: DOI: 10.1039/c9mh00051h

Hemocompatibility of super-repellent surfaces: current and future†

Sanli Movafaghi,[a] Wei Wang,[a] David L. Bark Jr.,[ab] Lakshmi P. Dasi,*[c] Ketul C. Popat*[ab] and Arun K. Kota*[abd]

Received 10th January 2019,
Accepted 30th April 2019

DOI: 10.1039/c9mh00051h

rsc.li/materials-horizons

Virtually all blood-contacting medical implants and devices initiate immunological events in the form of thrombosis and inflammation. Typically, patients receiving such implants are also given large doses of anticoagulants, which pose a high risk and a high cost to the patient. Thus, the design and development of surfaces with improved hemocompatibility and reduced dependence on anticoagulation treatments is paramount for the success of blood-contacting medical implants and devices. In the past decade, the hemocompatibility of super-repellent surfaces (*i.e.*, surfaces that are extremely repellent to liquids) has been extensively investigated because such surfaces greatly reduce the blood–material contact area, which in turn reduces the area available for protein adsorption and blood cell or platelet adhesion, thereby offering the potential for improved hemocompatibility. In this review, we critically examine the progress made in characterizing the hemocompatibility of super-repellent surfaces, identify the unresolved challenges and highlight the opportunities for future research on developing medical implants and devices with super-repellent surfaces.

1. Introduction

Blood-contacting medical implants and devices (*e.g.*, vascular grafts, stents, heart valves, left ventricular assist devices (LVADs), heart-lung machines, *etc.*) have saved or improved the quality of life for millions of patients. Despite their widespread use, all blood-contacting implants and devices have been shown to initiate inflammation, hemolysis, platelet activation, fibrosis and/or infection,[1,2] potentially leading to complications over

[a] Department of Mechanical Engineering, Colorado State University, Fort Collins, CO 80523, USA. E-mail: ketul.popat@colostate.edu, arun.kota@colostate.edu
[b] School of Biomedical Engineering, Colorado State University, Fort Collins, CO 80523, USA
[c] Department of Biomedical Engineering, The Ohio State University, Columbus, OH 43210, USA. E-mail: dasi.1@osu.edu
[d] Department of Chemical & Biological Engineering, Colorado State University, Fort Collins, CO 80523, USA

† Electronic supplementary information (ESI) available. See DOI: 10.1039/c9mh00051h

Lakshmi P. Dasi

Lakshmi P. Dasi received his PhD in Civil & Environmental Engineering from Gerogia Institute of Technology in 2004. In 2015, he joined the Department Biomedical Engineering at Ohio State University, where he currently serves as an Associate Professor. Prior to his current position at Ohio State University, he served as an Associate professor of Mechanical Engineering at Colorado State University from 2009 to 2015. His research interests include cardiovascular and biofluid Mechanics, fluid dynamics, biomaterials, biomechanics, Micro/Nanotechnology devices, heart valve prostheses, heart development and turbulence.

Ketul C. Popat

Ketul C. Popat received his PhD in Bioengineering from the University of Illinois at Chicago in 2003. He worked as a Post-doctoral Fellow in Biomedical Engineering at Boston University from 2003 to 2005. In 2007, he joined the Department of Mechanical Engineering and the School of Biomedical Engineering at Colorado State University, where he currently serves as an Associate Professor. Prior to joining Colorado State University, he was a Research Specialist in the Department of Physiology at the University of California, San Francisco. His research interests include biomaterials, tissue engineering and regenerative medicine.

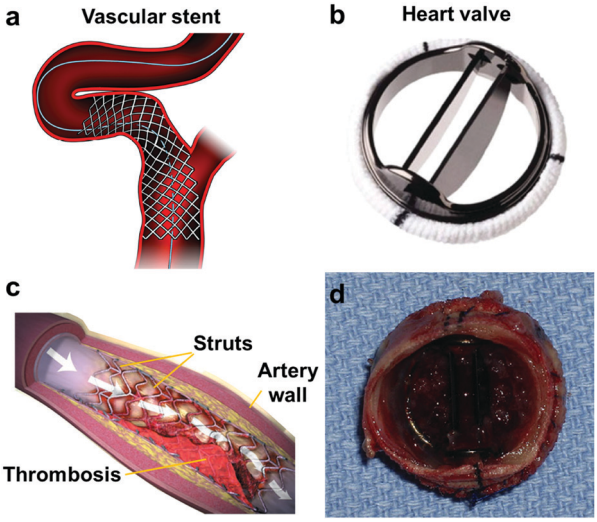

Fig. 1 A few examples of blood-contacting medical implants and devices: (a) vascular stent; reproduced with permission[76] © 2014 SAGE Publications and (b) heart valve; reproduced with permission[77] © 2015 Springer Nature. Typically, such implants and devices fail over the long term due to immunological events in the form of thrombosis and inflammation (c and d). Reproduced with permission[78,79] ©2007 Massachusetts Medical Society and © 2011 Elsevier.

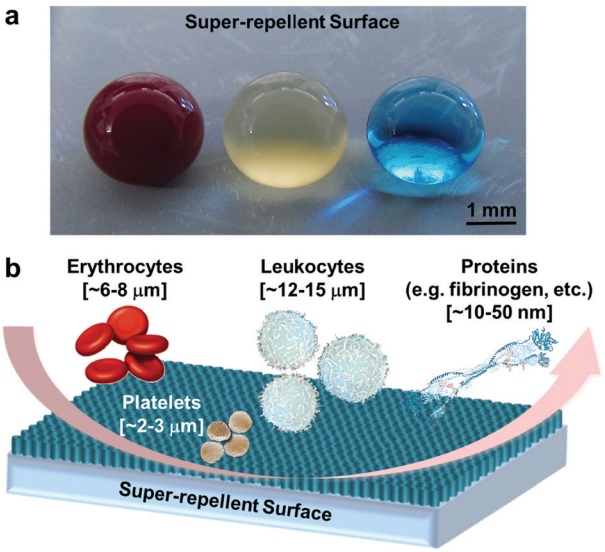

Fig. 2 (a) Droplets of blood, plasma and water beading up on a super-repellent surface. (b) Schematic (not drawn to scale) depicting the components of blood being "repelled" by a super-repellent surface due to the reduced blood–material contact area.

the long term (Fig. 1).[3,4] As a result, these implants and devices typically require anticoagulant, and sometimes antiplatelet therapies, at a high risk and a high cost to the patient.[5–7] These therapies can exhibit limited efficacy in dynamic blood flow environments,[8] while increasing the risk for bleeding, which at a minimum can result in a lower quality of life, and can also be fatal.[9] Therefore, there is a dire need for better hemocompatible materials with smart design features that could provide significant benefits for numerous patients.

The success of any blood-contacting medical device highly depends on the ability to control blood–material interactions, which in turn determines the hemocompatibility (*i.e.*, the tolerance of blood to materials).[10,11] Hemocompatibility is a broad and loosely defined term that is affected not only by different material properties such as surface chemistry,[12–18] surface texture,[19–23] surface wettability,[24–27] surface charge,[28–31] porosity[32,33] and surface modulus,[34–36] but also by different device design features.[37–43] In spite of the massive work devoted to improving hemocompatibility, the fabrication and design of hemocompatible materials, implants and devices for clinical applications has remained a great challenge in the biomaterials community.

In the past two decades, super-repellent surfaces (*i.e.*, surfaces that are extremely repellent to liquids)[44] have received considerable attention for their applications in anti-fouling,[45,46] self-cleaning,[47–52] liquid drag reduction,[53–55] chemical shielding,[56] icephobicity,[57–59] micro-robots,[60,61] anti-corrosion coatings,[62,63] enhanced dropwise condensation,[64–67] and controlled manipulation of liquid droplets.[68–71] Liquids can bead up on and easily roll off from super-repellent surfaces. More recently, super-repellent surfaces have been investigated for their hemocompatibility[25,72,73] because they significantly reduce the blood–material interfacial contact area, which in turn reduces the area available for protein adsorption and blood cell or platelet adhesion (Fig. 2). Further, super-repellent surfaces induce slip and significantly alter shear stresses at the blood–material interface, which in turn may reduce the overall damage to blood cells and platelets.[54,74,75] In this work, we critically examine the progress made in using super-repellent surfaces for improving hemocompatibility, and identify the potential challenges and opportunities. We provide our perspective on hemocompatibility and briefly discuss the biological responses ensuing from blood–foreign material interaction in Section 2. In Section 3, we review the common techniques for characterizing hemocompatibility and discuss how such experiments can be standardized. Subsequently, in Section 4, we discuss

Arun K. Kota

Arun K. Kota received his PhD in Mechanical Engineering from the University of Maryland in 2008. From 2009 to 2013, he worked as a Postdoctoral Fellow in the Department of Materials Science and Engineering at the University of Michigan. In 2013, he joined the Department of Mechanical Engineering at Colorado State University, where he currently serves as an Assistant Professor. His research interests include super-repellent surfaces, biocompatible surfaces, chemically patterned surfaces, stimuli-responsive surfaces, icephobic surfaces, droplet manipulation approaches and droplet fluid dynamics.

the underlying chemical and physical principles for the design and fabrication of super-repellent surfaces and provide a review of the studies on the interaction of blood with super-repellent surfaces, with particular emphasis on protein adsorption and blood cell interaction. Finally, we discuss the potential challenges and opportunities for improving hemocompatibility with super-repellent surfaces, in Section 5. Overall, this review aims to bridge the gap between materials scientists/engineers working on super-repellent surfaces and biomedical scientists/engineers working on hemocompatibility in an effort to pave the way for new and improved medical implants. To better facilitate this, the biological terms used in the context of blood–material interactions are described in Table S1 (ESI†).

2. Hemocompatibility: a description

The term ''hemocompatibility'' has been widely used for the past 50 years to describe materials, implants and devices that do not adversely interact with blood. However, hemocompatibility is not a very well-defined term and depends significantly on the type of device or application.[80] Adverse interactions with blood can refer to thrombosis (*i.e.*, clot formation) and/or inflammation (*i.e.*, an immune response), which are increasingly being considered interdependent.[81–83] Some studies relate hemocompatibility to the anti-thrombotic nature of a blood-contacting device, while others relate it to the anti-inflammatory response, and yet other studies relate it to a combination of anti-thrombotic and anti-inflammatory responses.[4,14,31,84–88] Furthermore, these responses vary significantly depending on the blood flow environment.

In order to thoroughly evaluate hemocompatibility of a material or a device, an in-depth and mechanistic understanding of the blood–material interactions is highly essential. At the core of initial hemocompatibility characterization is the resistance to interdependent – (1) thrombosis and (2) inflammation. So, how does a material initiate and propagate these responses? We aim to briefly answer this question in this section in the context of blood-contacting medical implants and devices (Fig. 3). Longer term events, such as endothelialization and intimal hyperplasia, are equally important, but will be excluded from the discussion for the sake of brevity.

2.1. Thrombosis

As recognized many years ago, thrombosis depends on the surface of the medical implant, the state of blood, and the flow environment.[89–94] The primary blood cell involved in thrombosis is a platelet. Normally, in humans, platelets travel through the blood circulation as inert cells. When platelets encounter an implant, they adhere to it, possibly activate and even aggregate.[95,96] The adhesion of platelets to an implant is facilitated by plasma proteins, specifically, fibrinogen and von Willebrand Factor (VWF), which adsorb on and serve as a bridge between the implant surface and the platelets. While fibrinogen is the primary binding protein utilized by platelets at lower wall shear rates (typically, $<600\ s^{-1}$), VWF is necessary

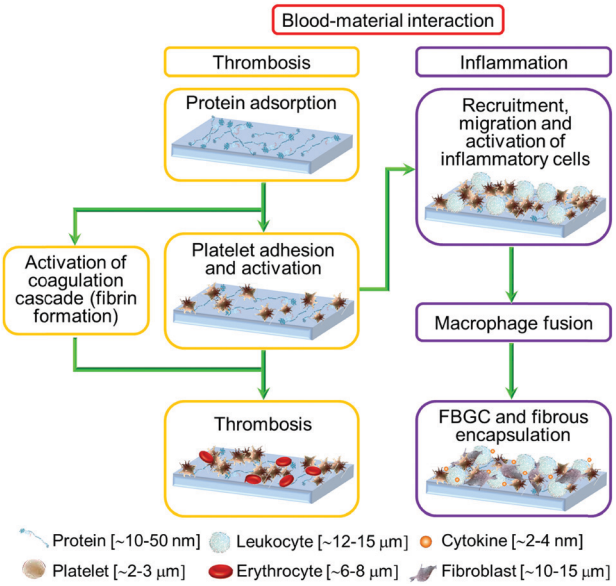

Fig. 3 A schematic (not drawn to scale) illustrating the biological responses ensuing from blood–foreign material interaction.

at higher wall shear rates.[97–99] Human serum albumin, the most abundant plasma protein that is relatively inert to the platelets, competes with fibrinogen and VWF for adsorption on the implant surface, and can reduce platelet adhesion by surface passivation.[100] Once platelets adhere to the implant surface, they can activate, depending on the protein configuration and the environment around the implant surface. Platelet activation is typically characterized by a change in shape of the platelets from a discoid to an amorphous form with projecting extensions. It also involves a conformational change in integrins on the surface of the platelets, which increases the affinity for binding with fibrinogen. Further release of α-granules from platelets[97,101] leads to exposure of membrane-bound proteins, while also releasing contents (*e.g.*, platelet activation agonists, VWF, *etc.*) from the platelet surface to the surrounding environment. This can promote the activation of the surrounding unactivated platelets. Additional platelets can then be recruited, leading to platelet–platelet binding, known as platelet aggregation. If sufficiently stimulated, platelets will also transition from a prothrombotic state to a procoagulant state.[102–104]

If flow is sufficiently slow (*i.e.*, at lower shear rates), the coagulation cascade can occur simultaneously, resulting in fibrin formation. Fibrin monomers result from the cleavage of fibrinogen by thrombin, which can be generated on the activated platelet surface.[105] Fibrin monomers can then assemble into protofibrils, which aggregate laterally to form fibers that crosslink to form a fibrin gel. The process of fibrin formation is complex, involving mass transport and multiple reactions that depend on the coagulant state, cellular activity, and fibrinolysis.[106,107] Fibrin, overall, aids in the stabilization of a thrombus.

2.2. Inflammation

Inflammation is the immune response process by which leukocytes protect the body from foreign objects, including implants.

Once platelets adhere to the implant surface (facilitated by plasma proteins), they can recruit leukocytes (*e.g.*, neutrophils, monocytes, lymphocytes *etc.*) involved in the innate immune system and encourage leukocyte migration and activation.[108] Neutrophils, the polymorphonuclear leukocytes, can form neutrophil extracellular traps (NETs), as a result of toll-like receptor 4 found on platelets.[109,110] NETs are composed of a meshwork of DNA fibers with a purpose of trapping microbes. NETs also capture platelets and can then stimulate thrombus formation.[111] Monocytes, the largest leukocytes, release inflammatory cytokines and chemokines (small cytokines) that provide signals for other cells to adhere and activate on the implant surface.[112–115] This subsequently results in acute inflammation, followed by chronic inflammation that further promotes monocyte differentiation into macrophages, intercellular communication and finally cell apoptosis. This cascade of events results in infiltration of lymphocytes and recruitment of fibroblasts from the surrounding tissue. Further, cytokines bind to cell surface receptors and either promote (pro-inflammatory) or impede (anti-inflammatory) intracellular function, intercellular communication and extracellular matrix deposition.[116,117] The resulting foreign body reaction (foreign body giant cells, FBGC) and fibrosis can lead to fibrous encapsulation of the implant, isolating it from the rest of the body. This natural wound healing response hinders tissue integration with the implant, thus affecting their long term efficacy in the body.[114]

In summary, thrombosis and inflammation occur through a series of steps that are initiated by protein adsorption and mediated by blood cell adhesion. So, the development of smart surface designs that minimize protein adsorption and blood cell adhesion can be greatly beneficial for blood-contacting medical implants and devices.

3. Characterization and standardization of hemocompatibility

Various characterization techniques have been developed to assess the hemocompatibility of materials, driven by the need for characterizing their safety and performance. An *in vitro* approach is to compare modified materials with unmodified controls of the same material. Here, we discuss a few *in vitro* tests that can be performed to assess the hemocompatibility. Note that this is not a comprehensive list and that the exact tests will need to be based on the context.

The degree of adsorption of relevant blood proteins can be assessed by protein labeling, *e.g.*, with radiolabels or fluorescent tags, with the assumption that the label exists on a known percentage of the adsorbing proteins. In addition to degree of protein adsorption, protein conformation also influences hemocompatibility. Protein conformation can be challenging to quantify, but approaches such as Fourier transform infrared spectrometric analysis, single-molecule electron transfer, *etc.* are being developed for this purpose.[118,119] Blood cell adhesion can be quantified either by counting the number of adherent cells or by measuring the area of adherent cells.[120] Other approaches include counting cells before and after contact with the surface, *e.g.*, with a hemocytometer. Platelet activation can be assessed in many ways including α-granule release, integrin $\alpha_{IIb}\beta_{III}$ conformational change and characterization of shape change *via* electron microscopy.[121] The former two can be assessed through immunolabeling. Assessing the propensity for coagulation can be a challenge since blood readily coagulates outside the body. Therefore, experiments must be performed immediately after drawing blood or may require an anticoagulant with a reversing agent. Various steps of the coagulation cascade can also be assessed. Cell death can be assessed through detection of phosphatidylserine exposure on the outer membrane leaflet of a cell using fluorescent tags.[122] Death occurs in platelets as they become highly activated, transitioning from a prothrombotic to a procoagulant state. Furthermore, hemolysis can also occur as a result of material contact with blood. Assays that quantify hemolysis typically measure the release of free hemoglobin from the lysed cells. Furthermore, the complement system, consisting of over 20 plasma proteins, plays a significant role in the body's defense mechanisms against infection and foreign objects (*e.g.*, implants) and supports the innate immune system and hence is important to evaluate using biochemical assays.[123]

Various standards (*e.g.*, ISO 10933-4, ASTM F2888) set by regulatory agencies provide guidance on how to investigate the hemocompatibility of medical implants and devices.[124] The guidelines describe appropriate methods for evaluation of blood–material interaction, however, they are dependent on the specific device or application and further, these standards continue to be malleable as science advances.[124–126] In addition, the complexity of blood–material interactions makes *in vitro* testing highly variable and testing is highly context dependent. For example, blood flow conditions, *e.g.*, static *vs.* dynamic or laminar *vs.* turbulent, alone can greatly impact *in vitro* and *in vivo* biological responses. Furthermore, timescales are an important consideration since implantable devices must remain effective as long as possible and could involve tissue growth on and around the device, while a short-term device may just need to resist an initial thrombotic and/or inflammatory response. Some implants may benefit from tissue growth (*e.g.*, endothelialization of bare metal stents), while others (*e.g.*, heart valve leaflets) benefit from prevention of tissue growth altogether. Certain vascular beds may also respond differently from others.

Overall, the context is very important when considering the hemocompatibility of a device. Standards set by regulatory agencies are for thorough and comprehensive investigation of implants, devices and drugs, rather than individual materials. Therefore, it is extremely difficult to define the term "hemocompatibility" in the general context of a material without referring to the medical device itself. Consequently, establishing a single worldwide standard for hemocompatibility of materials may be questionable.

4. Hemocompatibility of super-repellent surfaces

Super-repellent surfaces are extremely repellent (*i.e.*, highly non-wetting) to contacting liquids. Surface wettability (*i.e.*, the degree of spreading of a liquid on a solid surface),[127,128] which

is a function of both surface chemistry and surface texture, significantly influences hemocompatibility of materials, implants and devices.[24–27] The wettability of solid surfaces is typically characterized by two parameters, contact angle and contact angle hysteresis (*i.e.*, the difference between the advancing [maximum] and receding [minimum] contact angles).[129–131] Surfaces can be classified based on their water contact angles as hydrophilic (when they display contact angles $<90^\circ$ with water), hydrophobic (when they display contact angles $>90^\circ$ with water) and superhydrophobic (when they display contact angles $>150^\circ$ and contact angle hysteresis $<10^\circ$ with water). Typically, hydrophilic surfaces display lower blood protein adsorption and lower blood cell interaction (*i.e.*, adhesion and activation) compared to hydrophobic surfaces.[132–144] Unlike hydrophobic surfaces, superrepellent surfaces (*e.g.*, superhydrophobic surfaces) attracted significant attention because they display low blood protein adsorption and low blood cell interaction (as described in subsequent sections), which in turn leads to enhanced hemocompatibility.

4.1. Chemistry and physics of super-repellent surfaces

One of the first observations of super-repellency to water was on Lotus leaves and hence the term "Lotus effect" is commonly used to describe superhydrophobicity (Fig. 4a).[145–147] Detailed inspection of the Lotus leaves has established that appropriate surface chemistry and appropriate surface texture (and the associated physical principles) are the important factors leading to superhydrophobicity.[147–149] In this section, the underlying chemical and physical principles of super-repellent surfaces are discussed.

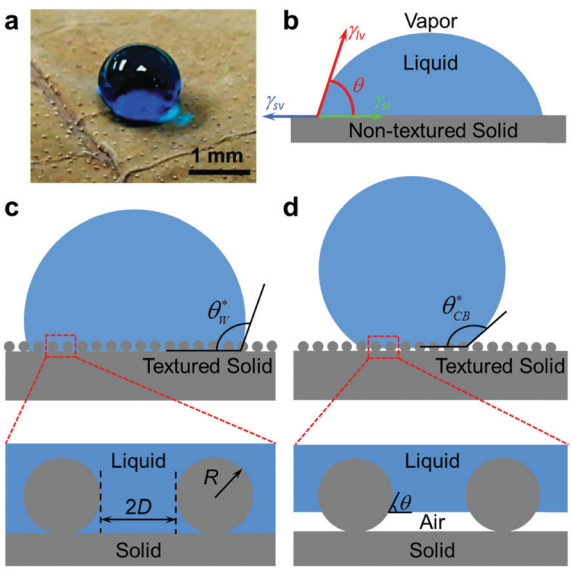

Fig. 4 (a) A droplet of water (dyed blue) beading up on a lotus leaf. Reproduced with permission.[130] © 2014 Nature Publishing Group. Schematic of a liquid droplet (b) on a non-textured solid surface, (c) in the Wenzel state on a textured solid surface, and (d) in the Cassie–Baxter state on a textured solid surface. Note: θ^*, apparent contact angle; θ, Young's contact angle; R, radius of the feature; D, half the inter-feature spacing.

The primary measure of wetting of a liquid on a non-textured (*i.e.*, smooth) solid surface (Fig. 4b) is the equilibrium (or Young's) contact angle θ, given by Young's equation:[150]

$$\cos\theta = \frac{\gamma_{sv} - \gamma_{sl}}{\gamma_{lv}} \quad (1)$$

Here, γ_{sv}, γ_{sl} and γ_{lv} are the solid–vapor interfacial tension, the solid–liquid interfacial tension and the liquid–vapor interfacial tension, respectively. γ_{sv} is also known as the solid surface energy and γ_{lv} is also known as the liquid surface tension. Young's equation (eqn (1)) implies that the contact angle θ increases with decreasing solid surface energy γ_{sv}. In other words, surfaces with low solid surface energy tend to display higher contact angles.[130] So, materials with low solid surface energy (*e.g.*, hydrocarbons with $\gamma_{sv} \approx 20$–35 mN m^{-1} and fluorocarbons with $\gamma_{sv} \approx 10$–20 mN m^{-1})[151] are preferred to design surfaces with high contact angles. Even with the lowest solid surface energy materials known, the maximum possible contact angle of water on a non-textured surface is about 130°.[152–154] In order to obtain higher water contact angles, surface texture is essential.

When a droplet contacts a textured (*i.e.*, rough) solid surface, it displays an apparent contact angle θ^*, which is different from the Young's contact angle θ. On a textured surface, the droplet can adopt either the Wenzel[155] state or the Cassie–Baxter state[156] to minimize its overall free energy. In the Wenzel state, the droplet penetrates into the surface asperities and fully wets the solid surface (Fig. 4c). In this state, the apparent contact angle θ^* can be estimated with the Wenzel relation:[155]

$$\cos\theta^* = r\cos\theta \quad (2)$$

Here, r is the surface roughness defined as the ratio of the actual surface area to the projected surface area. Since $r > 1$, the presence of surface roughness amplifies the wetting behavior of surfaces in the Wenzel state (*i.e.*, $\theta^* \ll 90^\circ$ if $\theta < 90^\circ$ and, $\theta^* \gg 90^\circ$ if $\theta > 90^\circ$). Typically, low surface tension liquids (*e.g.*, oils and alcohols) display Young's contact angle $\theta < 90^\circ$ on most solid surfaces. So, low surface tension liquids tend to display very low apparent contact angles (*i.e.*, $\theta^* \ll 90^\circ$) in the Wenzel state.

In the Cassie–Baxter state, there are air pockets trapped between the solid (Fig. 4d) and the liquid and θ^* can be estimated using the Cassie–Baxter relation:[156]

$$\cos\theta^* = f_{sl}\cos\theta + f_{lv}\cos\pi = f_{sl}\cos\theta - f_{lv} \quad (3)$$

Here, f_{sl} is solid–liquid area fraction and f_{lv} is the liquid–air area fraction underneath the liquid droplet.[157] It is evident from the Cassie–Baxter relation (eqn (3)) that it is possible to have an apparent contact angle $\theta^* \gg 90^\circ$ not only for $\theta > 90^\circ$ but also for $\theta < 90^\circ$, if the liquid–air area fraction f_{lv} is sufficiently high and the solid–liquid area fraction f_{sl} is sufficiently low.[158] In other words, the Cassie–Baxter state can lead to very high contact angles for liquids with both high and low surface tensions.

Contact angle hysteresis $\Delta\theta^*$ (the difference between the advancing and receding contact angles; Fig. 5a), which is the

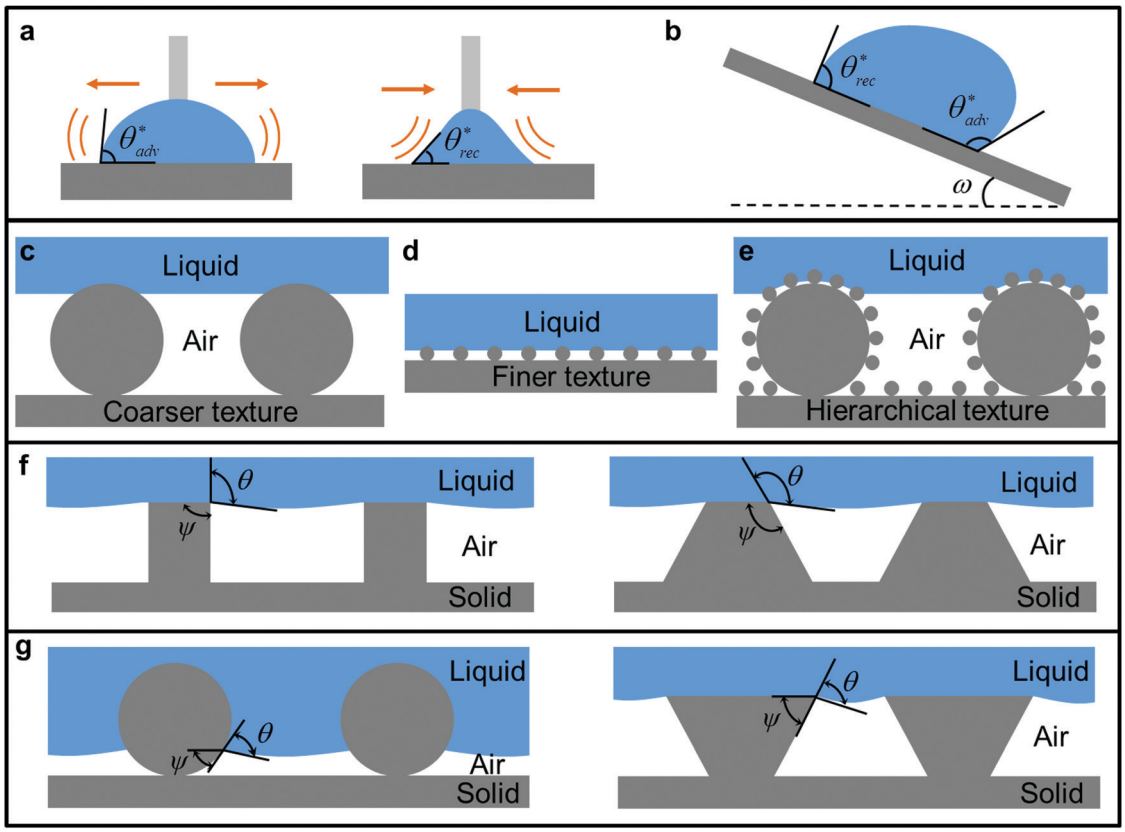

Fig. 5 Schematic illustrating (a) the advancing (the maximum) and receding (minimum) contact angles on a solid surface, and (b) a liquid droplet sliding on a tilted surface with the roll off angle of ω. Schematics of a liquid droplet in the Cassie–Baxter state on (c) a coarser textured surface, (d) a finer textured surface, and (e) a hierarchically structured surface, respectively. Schematics of a liquid droplet on (f) concave textures with $\psi \geq 90^\circ$ showing a liquid with $\theta > 90^\circ$ in the Cassie–Baxter state, and (g) convex (re-entrant) textures with $\psi < 90^\circ$ showing a liquid with $\theta < 90^\circ$ in the Cassie–Baxter state. Note: ψ, local texture angle.

second important parameter for characterizing surface wettability, primarily arises from physical and chemical heterogeneity of the surface.[130,159,160] It is related to the energy barriers that oppose the movement of a liquid droplet along a solid surface. In other words, contact angle hysteresis characterizes the resistance to droplet movement.[159,160] Since the solid–liquid area fraction f_{sl} in the Cassie–Baxter state is low, it results in lower solid–liquid interaction and lower contact angle hysteresis $\Delta\theta^*$.[161,162] Consequently, the Cassie–Baxter state facilitates high mobility of the contacting liquid droplets and leads to a low roll off angle (*i.e.*, the minimum angle ω by which the surface must be tilted for the droplet to roll off) on super-repellent surfaces (Fig. 5b). Therefore, the Cassie–Baxter state is preferred for designing super-repellent surfaces, which display high contact angles as well as low contact angle hysteresis (or low roll off angles).[161,162] Furthermore, hierarchically structured surfaces (*i.e.*, surfaces that possess more than one scale of texture; a finer length scale texture on an underlying coarser length scale texture) can lead to further decrease in solid–liquid interfacial area and interaction (Fig. 5c–e)[130,143] and thereby enhance super-repellency.

Not all types of textures can lead to a stable Cassie–Baxter state for a contacting liquid. To understand this, consider two types of textures shown in Fig. 5f and g, with the same solid surface energy. The textures in Fig. 5f are concave (texture angle $\psi \geq 90^\circ$), while the textures in Fig. 5g are convex ($\psi < 90^\circ$). In both cases, any liquid adopting the Cassie–Baxter state will locally display the Young's contact angle. A stable Cassie–Baxter state is possible only when $\theta \geq \psi$.[56,130,143,163–165] If $\theta < \psi$, the net traction due to capillary force is downward on the liquid–vapor interface, which leads to the Wenzel state. Consequently, when a liquid droplet comes in contact with a concave texture, the Cassie–Baxter state is only possible with high surface tension liquids (*e.g.*, water) with high Young's contact angles ($\theta > 90^\circ$).[165,166] In other words, concave textures can only lead to superhydrophobic surfaces. On the other hand, when a liquid droplet comes in contact with a convex (or re-entrant) texture, the Cassie–Baxter state is possible for both high surface tension liquids with high Young's contact angles and low surface tension liquids with low Young's contact angles. In other words, a concave texture can lead to superomniphobic surfaces (*i.e.*, surfaces that are extremely repellent to virtually any liquid).

Convex (or re-entrant) texture is necessary, but not sufficient for the formation of the Cassie–Baxter state for contacting liquids.[165,167] Typically, the Cassie–Baxter state is a metastable state.[165,167] When a sufficiently high pressure is applied on a

liquid in the Cassie–Baxter state, regardless of the type of texture, the liquid will breakthrough (*i.e.*, permeate and fully wet the protrusions), thereby transitioning to the Wenzel state. The breakthrough pressure $P_{breakthrough}$ is the minimum pressure that can force such a transition from the Cassie–Baxter state to the fully wetted Wenzel state. The breakthrough pressure $P_{breakthrough}$ can be determined from a force balance at the liquid–air interface. Typically, higher surface tension liquids and/or surface textures with smaller inter-feature spacings have higher $P_{breakthrough}$.[165,167] Optimal super-repellent surfaces need to simultaneously display high $P_{breakthrough}$ and high apparent contact angles θ^* with the contacting liquid. High θ^* can be obtained from high liquid–air area fraction f_{lv}. One way of obtaining high f_{lv} is to design a texture with large inter-feature spacing. However, larger inter-feature spacings result in lower $P_{breakthrough}$. In order to obtain high $P_{breakthrough}$ without compromising high θ^*, it is essential to decrease the length scale of the texture. Consider a microstructure with $f_{lv,micro}$ and $P_{breakthrough,micro}$ and a nanostructure with $f_{lv,nano}$ and $P_{breakthrough,nano}$. If the nanostructure is designed with $f_{lv,micro} = f_{lv,nano}$, it will display a θ^* similar to that obtained with the microstructure, but the nanostructure will have $P_{breakthrough,nano} \gg P_{breakthrough,micro}$ due to smaller inter-feature spacing. In this manner, by designing textures on smaller length scales (*e.g.*, nanostructure) with high liquid–air area fraction, one can obtain super-repellent surfaces that simultaneously display high breakthrough pressures and high apparent contact angles.

4.2. Super-repellent surfaces: blood wettability

In many studies on the hemocompatibility of super-repellent surfaces, the wettability of the surface was characterized with water contact angles. However, superhydrophobic surfaces may not display high contact angles and more importantly, very low roll off angles with blood. This is because blood surface tension ($\gamma_{lv} \approx 56$ mN m^{-1})[168] is lower compared to water surface tension ($\gamma_{lv} \approx 72$ mN m^{-1}). In studying the hemocompatibility of super-repellent surfaces, perhaps a better way of characterizing the surface wettability would be to report the contact angles and roll off angles (or contact angle hysteresis) of blood or plasma on the super-repellent surface. In this context, superhemophobic surfaces can be defined as surfaces that display very high contact angles ($>150^\circ$) and very low roll off angles ($<10^\circ$) with blood. It must be emphasized here that reporting just the static contact angle or the apparent advancing contact angle of blood or plasma does not adequately describe the super-repellency to blood. The apparent receding contact angle, contact angle hysteresis or roll off angle of blood or plasma on the super-repellent surface must be measured and reported because they are useful to understand the heterogeneity and blood mobility on the surface. It is also important to estimate the breakthrough pressure of blood or plasma on the super-repellent surface because it is useful in determining the robustness of the Cassie–Baxter state.

Typically, super-repellent surfaces are considered to enhance hemocompatibility because blood adopts the Cassie–Baxter state with low blood–material contact area (*i.e.*, low solid–liquid area fraction f_{sl}), thereby greatly minimizing the available binding sites for blood protein adsorption and blood cell–material interaction. As described previously (see Section 4.1), optimal super-repellent surfaces with textures on smaller length scales (*e.g.*, nanostructure) and high liquid–air area fraction (or low solid–liquid area fraction) can not only enhance hemocompatibility, but also improve longevity of super-repellent surfaces when immersed in blood (due to high breakthrough pressure) and impede blood cells from intruding into the surface topography.

4.3. Blood protein adsorption on super-repellent surfaces

Plasma protein adsorption can be affected by surface wettability as well as protein parameters such as primary structure, size, structural stability, *etc.*[25,169] Most reports in the literature have shown that the protein adsorption on superhydrophobic surfaces (*i.e.*, in the Cassie–Baxter state) is significantly lower than that on non-textured surfaces and fully wetted textured surfaces (*i.e.*, in the Wenzel state). For example, Ballester-Beltrán *et al.*[170] fabricated a superhydrophobic surface, consisting of a micro and nanotextured (*i.e.*, hierarchically structured) polystyrene (PS) ($\gamma_{sv} \approx 35$ mN m^{-1}) surface, using a phase separation method. They investigated the adsorption of fibronectin on their superhydrophobic PS surface and compared it with that on a non-textured PS surface. Their results indicate about 60% reduction in the amount of adsorbed fibronectin on a superhydrophobic PS surface compared to the non-textured PS surface, which led to a reduction in focal adhesion and actin organization (Fig. 6a). Furthermore, they reported fibronectin adsorption in an altered conformation and denaturation of the protein upon adsorption on the superhydrophobic PS surface. Pernites *et al.*[171] combined PS layering and cyclic voltammetry-electropolymerization of polythiophene to fabricate surfaces with switchable wettability and achieved superhydrophobicity with undoped polythiophene film. They observed the inhibition of fibrinogen adsorption on their superhydrophobic surfaces (about 85% reduction in the change in delta frequency Δf, a measure of protein adsorption) compared to a fully wetted textured surface. Zhao *et al.*[172] prepared hierarchically structured silica surfaces, with varying surface roughness (*i.e.*, single-, dual-, and triple-scale) using a layer-by-layer particle deposition approach. Furthermore, the surfaces were treated with 1*H*,1*H*,2*H*,2*H*-perfluorodecyl trichlorosilane ($\gamma_{sv} \approx 15$ mN m^{-1}) *via* chemical vapor deposition to induce superhydrophobicity. They reported that dual- and triple-scale structured superhydrophobic surfaces exhibited significantly reduced bovine serum albumin adsorption (up to 90% decrease compared to glass surface). In these studies, the reduced protein adsorption on superhydrophobic surfaces has been attributed to the lower contact area between the surface and the liquid medium containing the proteins.

On the other hand, Koc *et al.*[173] showed that not all superhydrophobic surfaces lead to lower protein adsorption compared to non-textured surfaces. They used a phase separation method to fabricate microstructured ($\sim$4 μm) sol–gel materials, nanostructured ($\sim$800 nm) sol–gel materials and nanostructured ($\sim$10 nm) copper–oxide filaments. These surfaces were chemically modified with hydrocarbon (octyltriethoxysilane; $\gamma_{sv} \approx 25$ mN m^{-1}) or fluorocarbon chemistry to obtain superhydrophobicity.

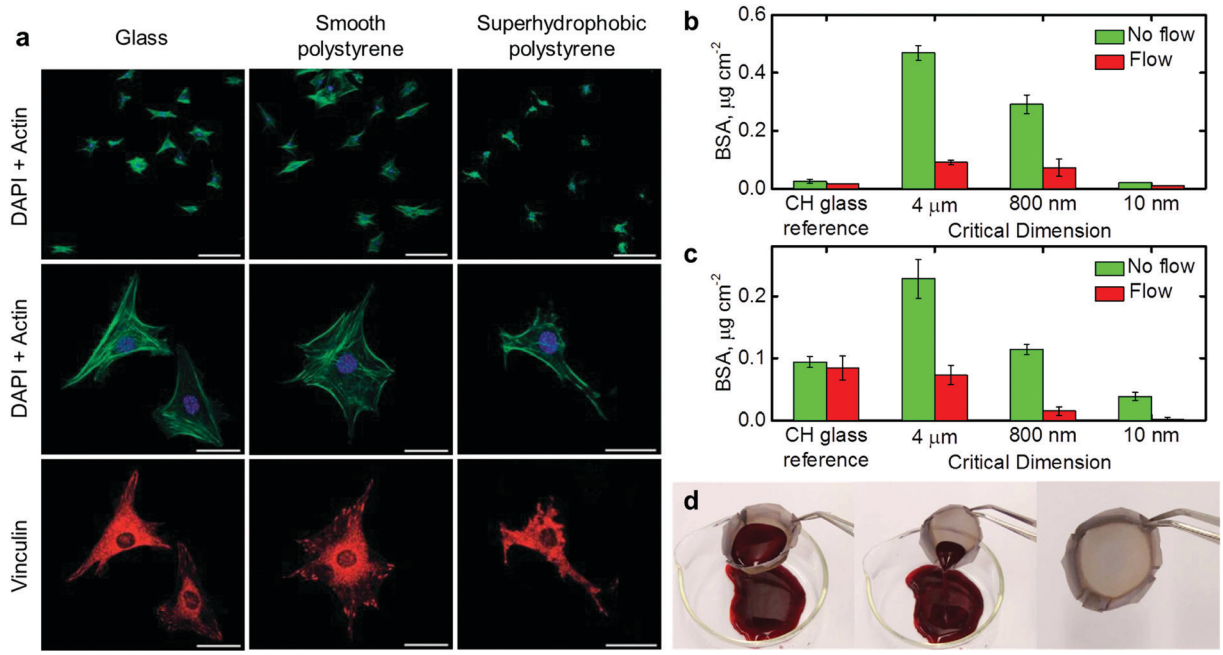

Fig. 6 (a) F-actin cytoskeleton (first and second rows) and distribution of focal adhesion protein, vinculin (third row), on control glass, smooth polystyrene and superhydrophobic polystyrene substrates. Nuclei were counterstained with 4,6-diamidino-2-phenylindole (DAPI). The scale bars represent 150 μm, 30 μm and 30 μm for the first, second and third rows, respectively. Reproduced with permission.[170] © 2011 Royal Society of Chemistry. Protein (BSA) adsorption on micro-scale and nano-scale surfaces modified with (b) hydrocarbon chemistry and (c) fluorocarbon chemistry, under static and flow conditions. Adapted with permission.[173] © 2008 Royal Society of Chemistry. (d) A series of images showing the repellency of superomniphobic steel mesh to whole human blood. Reproduced with permission.[175] © 2013 Nature Publishing Group.

They investigated the adsorption of bovine serum albumin on each of their superhydrophobic surfaces and compared it with that on a hydrophobic non-textured glass surface. For hydrocarbon surface chemistry, they showed that microstructured and nanostructured sol–gel superhydrophobic surfaces have about 95% and 90% higher protein adsorption, respectively, compared to the hydrophobic non-textured glass surface (*i.e.*, glass modified with hydrocarbon surface chemistry; Fig. 6b). They reported a similar trend for fluorocarbon surface chemistry (Fig. 6c). However, the protein adsorption on nanostructured copper oxide filaments was about the same (for hydrocarbon surface chemistry) or lower (about 60% reduction for fluorocarbon surface chemistry) compared to a hydrophobic non-textured glass surface (Fig. 6b and c). While the underlying reasons for the increase or decrease in protein adsorption on different superhydrophobic surfaces are not clear, one possible step towards explaining the differences could be through characterizing the advancing and receding contact angles as well as the breakthrough pressures of the different superhydrophobic surfaces using the relevant biological liquid (*e.g.*, blood or plasma or the protein solution) rather than water.

There are very few studies that have investigated the blood protein adsorption on super-repellent surfaces while characterizing the wettability and/or super-repellency of the surface using blood. Bartlet *et al.*[174] fabricated superhemophobic titania nanotube surfaces *via* electrochemical anodization followed by surface modification with a fluorocarbon (heptadecafluoro-1,1,2,2-tetrahydrodecyl trichlorosilane; $\gamma_{sv} \approx 10$ mN m^{-1}) chemistry. They reported that the adsorption of human serum albumin and human fibrinogen proteins on superhemophobic surfaces was lower compared to unmodified titania surfaces. Paven *et al.*[175] fabricated a superomniphobic membrane by coating stainless steel meshes with fluorinated (trichloro(1*H*,1*H*,2*H*,2*H*-perfluorooctyl)silane)silica particles (Fig. 6d). Their results indicate that the human blood protein adsorption on superomniphobic surfaces after 24 h was inhibited (by more than 95%) compared to that on bare steel mesh after 6 h.

In summary, most prior studies indicate that super-repellent surfaces, especially those with finer texture (*e.g.*, nanostructure) and those displaying superhemophobicity or superomniphobicity, show significantly lower blood protein adsorption compared to non-textured surfaces and fully wetted textured surfaces. However, it is difficult to compare the degree of blood protein adsorption on super-repellent surfaces across different studies due to multiple reasons. First, different studies have reported the degree of protein adsorption on super-repellent surfaces using different proteins (and their concentrations). Second, different studies have employed different control surfaces in reporting the change in the degree of protein adsorption. Third, the rough texture of super-repellent surfaces makes quantitative comparison more challenging. Fourth, it has been shown that measurement with different protocols can lead to different degrees of protein adsorption, depending on labeling efficiency and possibility of blocking binding domains with an antibody. For example, Leibner *et al.*[176] fabricated superhydrophobic surfaces using expanded polytetrafluoroethylene (ePTFE) ($\gamma_{sv} \approx 20$ mN m^{-1}).

They investigated the adsorption of human serum albumin on superhydrophobic ePTFE using two different methods, radiometry (I-labeled human serum albumin) and electrophoresis. They reported that the amount of adsorbed protein is four times higher with electrophoresis compared to radiometry. For all of these reasons, while comparing the trends is reasonable, one must be very cautious in comparing the absolute values of the degree of protein adsorption across studies. In order to facilitate comparison across studies, it may be prudent to characterize the degree of adsorption of multiple common and relevant blood proteins (*e.g.*, fibrinogen, fibronectin, albumin, VWF *etc.*) on carefully chosen control surfaces that are relevant in the context of the application.

4.4. Blood cell interaction with super-repellent surfaces

Similar to blood protein–surface interaction, blood cell–surface interaction is also strongly dependent on surface wettability and the cell type. Many reports in the literature claim that the blood cell adhesion on superhydrophobic surfaces is significantly lower than that on non-textured surfaces. For example, Li *et al.*[177] fabricated superhydrophobic surfaces using micro-textured polypropylene (PP) surfaces *via* a solvent–nonsolvent technique. By comparing the whole blood interaction with smooth and superhydrophobic PP, they indicated that the rupture and adhesion of red blood cells are remarkably reduced on the superhydrophobic PP compared to the smooth PP. Bark *et al.*[178] fabricated superhydrophobic surfaces by spray coating a commercially available water repellent coating, Ultra-Ever Dry®. They indicated that hierarchically structured superhydrophobic surfaces resulted in lower leukocyte adhesion compared to non-textured hydrophobic surfaces (Fig. 7a–d). In these studies, the reduced cell adhesion on superhydrophobic surfaces has been attributed to the lower contact area between the surface and the liquid medium containing the cells.

Several studies have investigated platelet adhesion and activation, both qualitatively and quantitatively, on superhydrophobic surfaces. Sun *et al.*[179] fabricated superhydrophobic surfaces by dip-coating aligned carbon nanotube films with fluorinated polycarbonate urethane (FPCU). They reported almost no platelet adhesion and activation on their superhydrophobic films compared to the non-textured FPCU films (Fig. 7e–h). Mao *et al.*[180] fabricated single length scale and hierarchical superhydrophobic PS nanotube films by alumina templating. They showed that the adhered and activated platelets are the lowest on hierarchical superhydrophobic PS nanotube films. Ye *et al.*[26] prepared polydimethylsiloxane (PDMS) based superhydrophobic surfaces using femtosecond laser ablation and soft lithography. They showed that fewer platelets adhered and activated on the superhydrophobic PDMS surfaces compared to non-textured PDMS surfaces. Hoshian *et al.*[181] fabricated a PDMS based superhydrophobic flexible tube using atomic layer deposition assisted sacrificial etching (Fig. 8a). They reported no platelet adhesion on the superhydrophobic surface compared to many adhered and activated platelets on control surfaces (*i.e.*, non-textured titania and PDMS surfaces).

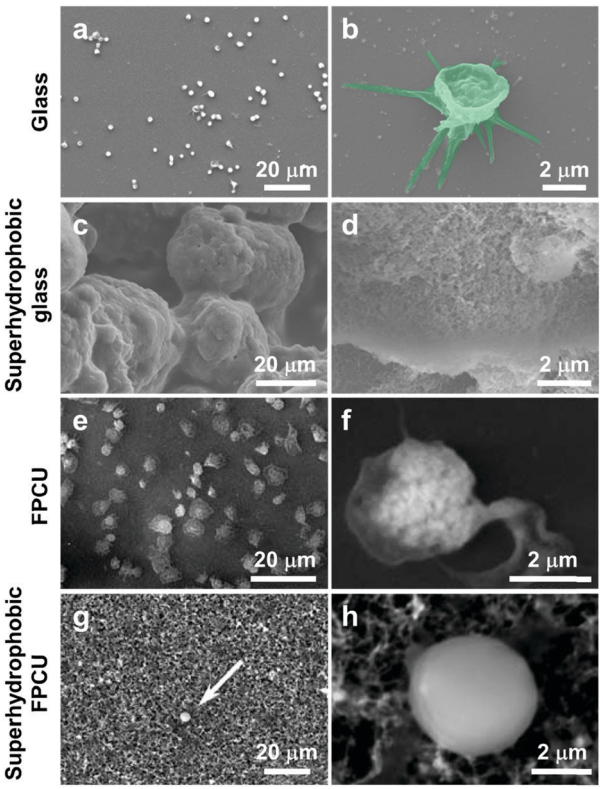

Fig. 7 SEM images showing platelet adhesion and activation on glass (a and b) and glass with a hierarchical superhydrophobic coating (c and d). Reproduced with permission.[178] © 2017 Springer. SEM images showing platelet adhesion and activation on non-textured FPCU films (e and f) and nanostructured superhydrophobic FPCU film. Reproduced with permission.[179] © 2005 Wiley.

In addition to the qualitative investigation of platelet adhesion discussed above, there have been several quantitative investigations. Khorasani *et al.*,[182] fabricated PDMS-based superhydrophobic surfaces using CO_2-pulsed-laser ablation. They reported about 87% reduction in the number of adhered platelets and almost no platelet activation on superhydrophobic surfaces compared to non-textured PDMS surfaces. Zhou *et al.*[183] fabricated PDMS-based superhydrophobic surfaces consisting of micro-pillars and nano-grooves using soft lithography. They showed about 80% and 98% reduction in the number of adhered platelets for superhydrophobic PDMS micro-pillars and hydrophobic PDMS nano-grooves, respectively, compared to a non-textured PDMS surface. Zhao *et al.*[172] investigated the platelet adhesion and activation on hierarchically structured superhydrophobic silica surfaces modified with fluorocarbon surface chemistry (1*H*,1*H*,2*H*,2*H*-perfluorodecyl trichlorosilane). They reported that only a few platelets adhered to single length scale and dual length scale superhydrophobic surfaces over an area of 20 μm by 20 μm, corresponding to about 65% and 85% reduction in the number of adhered platelets, respectively, compared to an unmodified glass surface. Furthermore, they reported that platelet adhesion on triple length scale superhydrophobic surfaces was nearly completely suppressed (about 90% reduction). Moradi *et al.*[184] used laser ablation to fabricate superhydrophobic titanium surfaces

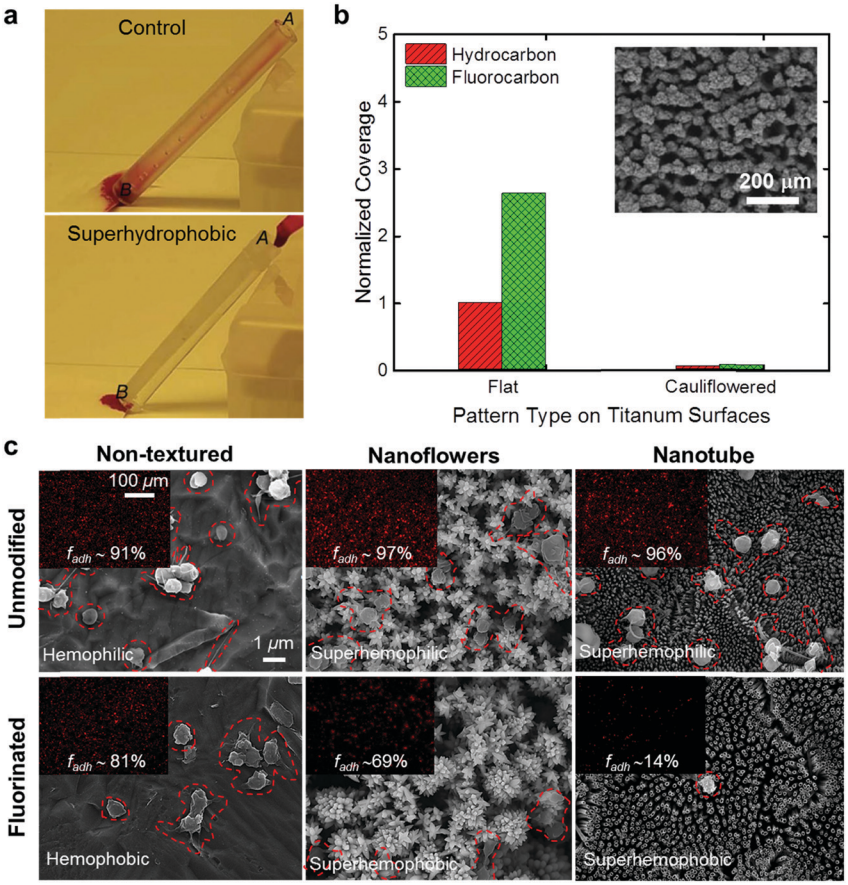

Fig. 8 (a) Images showing a blood droplet passing through a non-textured PDMS/titania tube (top image) and a superhydrophobic PDMS/titania tube (bottom image). Reproduced with permission.[181] © 2017 Nature Publishing Group. (b) Normalized platelet adhesion on different titanium surfaces. Inset shows an SEM image of the cauliflower-like texture of the surface. Adapted with permission.[184] © 2016 American Chemical Society. (c) SEM images showing platelet activation (enclosed by dotted lines in red) on titania surfaces. Insets show fluorescence microscopy images depicting platelet adhesion. Reproduced with permission.[185] © 2017 Wiley.

with cauliflower-like surface morphology and different surface modifications (*i.e.*, with adsorbed hydrocarbons and with a fluorinated silane). For both hydrocarbon and fluorocarbon surface chemistries, they observed that the superhydrophobic titanium surfaces resulted in 95% lower area of adhered platelets compared to non-textured titanium surfaces (Fig. 8b). They reported a similar trend for superhydrophobic stainless steel surfaces. In these studies, the reduced platelet adhesion and activation on superhydrophobic surfaces has been attributed to the low contact area between the surface and blood plasma.

Virtually all studies that investigated platelet adhesion and activation on superhydrophobic surfaces have characterized the surface wettability with water rather than blood or plasma. In contrast, Movafaghi *et al.*[185] characterized platelet adhesion and activation on superhemophobic titania surfaces with nanotube and nanoflower surface morphologies fabricated *via* hydrothermal synthesis and electrochemical anodization, respectively, and modified with fluorinated silane. They reported a 12% and 67% reduction in the area of adhered platelets on nanoflower and nanotube morphologies, respectively, compared to non-textured, fluorinated titania surfaces (Fig. 8c). They reported a similar trend in platelet activation as well. They attributed the lower platelet adhesion and activation on the nanotube morphology to lower inter-feature spacing and higher breakthrough pressure of blood or plasma (*i.e.*, a robust Cassie–Baxter state) compared to the nanoflower morphology. It may also be possible that the lower inter-feature spacing has impeded the intrusion of platelets more effectively.

In summary, almost all prior studies indicate that super-repellent surfaces show significantly lower platelet adhesion and activation compared to non-textured surfaces. However, similar to blood protein adsorption, comparison of blood cell interaction with super-repellent surfaces across different studies is a challenge due to multiple reasons. First, different studies have employed different control surfaces in reporting the change in blood cell interaction with super-repellent surfaces. Second, different studies used blood plasma with different platelet densities (*e.g.*, platelet-rich plasma or platelet-poor plasma as well as the differences that arise due to donor-to-donor variation). Third, while some studies are quantitative (desirable), others are only qualitative in characterizing blood cell interaction with super-repellent surfaces. Fourth, while some quantitative studies report the number of platelets adhered per unit area, other quantitative studies report the area fraction of the adhered platelets. Fifth, the

rough super-repellent surfaces make quantitative comparison more challenging. For all of these reasons, similar to blood protein adsorption, while comparing the trends is reasonable, one must be very cautious in comparing the absolute values of blood cell interaction measurements (*e.g.*, degree of platelet adhesion) and it may be prudent to carefully choose control surfaces that are relevant in the context of the application.

5. Hemocompatibility of super-repellent surfaces: challenges and opportunities

Investigating the hemocompatibility of super-repellent surfaces continues to be an active area of research because of its potential impact on a wide range of medical implants and devices. However, there are significant challenges, which are great opportunities for further research, as discussed below:

5.1. Mechanistic studies

Most studies on evaluating the hemocompatibility of super-repellent surfaces have investigated only the first few events (*e.g.*, protein adsorption, platelet adhesion and activation *etc.*) of the thrombotic response. However, evaluating single end-points in the blood-clotting cascade is not sufficient. To obtain a mechanistic understanding, the influence of different solid–liquid area fractions and different surface morphologies of the super-repellent surfaces on each single event in thrombotic and inflammatory responses should be investigated in detail. Clearly understanding the underlying mechanisms will allow materials scientists to better tune the texture and chemistry of the super-repellent surfaces for favorable interactions with blood.

5.2. Dynamic testing

Most studies on the hemocompatibility of super-repellent surfaces have characterized the interaction with blood under static conditions (*i.e.*, without blood flow). A few exceptions are Koc *et al.*[173] investigating the removal of adsorbed protein under flow (Fig. 6b and c) and Lai *et al.*[186] investigating the hemolysis rate under flow. The interaction of blood with the super-repellent surfaces under hemodynamic conditions (*e.g.*, unfolding of VWF, platelet adhesion, shear-dependent platelet activation, transport of coagulation factors and platelet agonists, such as ADP, thrombin, and thromboxane, *etc.* under flow)[187–190] can be significantly different from the static conditions. Since most practical materials, implants and devices experience hemodynamic conditions, it is essential to evaluate the hemocompatibility under relevant dynamic conditions (*e.g.*, blood flow rate, wall shear stress, pulsatile flow *etc.*) in the context of the application.[191]

5.3. Longevity

Practical application of super-repellent surfaces in blood-contacting medical implants and devices requires longevity of the Cassie–Baxter state (*i.e.*, air pockets). In order to avoid the loss of air pockets by dissolution of air into the blood or by breakthrough of blood into the texture, one strategy is to employ textures with as small an inter-feature spacing as possible (*e.g.*, sub-micron inter-feature spacings). In addition to offering very high breakthrough pressures, super-repellent surfaces with extremely small inter-feature spacings have the potential to offer virtually infinite lifetimes for the air pockets.[192–194] Furthermore, such surface textures can impede blood cells from intruding into the surface topography, which can potentially reduce blood cell adhesion, leading to improved hemocompatibility. Most studies have investigated the hemocompatibility of super-repellent surfaces for relatively short time scales (typically no more than a few minutes to hours) and there is a great need for more prolonged studies (over days, weeks and months).

5.4. Mechanical durability

Practical application of super-repellent surfaces in blood-contacting medical implants and devices also requires mechanical durability of the texture. While the number of reports on durable super-repellent surfaces continues to increase,[195–199] mechanical durability of super-repellent surfaces, especially against shear stresses in solid abrasion, continues to be a significant challenge. However, for certain blood-contacting applications (*e.g.*, mechanical heart valves, stents *etc.*), the primary shear stresses are those imposed by flowing blood, which may be more forgiving than solid abrasion. In such cases, super-repellent surfaces with sufficient mechanical durability may be viable. Regardless, there is a significant need for improving the mechanical durability (*e.g.*, by using monolithic textures of materials with high deformability and/or self-healing ability).

5.5. Benign surface chemistry

Many studies investigating the hemocompatibility of super-repellent surfaces have employed long chain fluorocarbon surface chemistry due its low solid surface energy. However, long chain fluorocarbon materials are rapidly being phased out by environmental agencies across the world because of the growing concerns regarding their negative environmental impacts (*e.g.*, non biodegradable) and biological impacts (*e.g.*, bioaccumulation). Consequently, future work should focus on employing benign surface chemistries that are non-toxic and non-bioaccumulative.

5.6. *In vivo* testing

Most studies investigating the hemocompatibility of super-repellent surfaces have focused on *in vitro* tests. However, to truly design and develop effective implantable medical devices, future studies should earmark more *in vivo* tests in animal models and eventually human clinical trials.

6. Conclusions

Hemocompatibility of super-repellent surfaces has been extensively investigated in the past decade and continues to be an active area of research because the reduced contact area

between blood and super-repellent surfaces offers the potential for improved hemocompatibility. In this review, we discussed the biological responses ensuing from blood–foreign material interaction as well as the chemistry and physics of super-repellent surfaces with the aim of better elucidating the potential interactions between super-repellent surfaces and blood. We also presented the recent studies on the blood protein adsorption and blood cell interaction with super-repellent surfaces and emphasized the need for careful and thorough characterization of super-repellent surfaces and their hemocompatibility. Finally, we presented the current challenges in developing medical implants and devices with super-repellent surfaces. While these challenges constitute significant opportunities for research and an exciting future, the nature of these challenges underscores the need for highly interdisciplinary teams of scientists and engineers to tackle them.

Conflicts of interest

There are no conflicts to declare.

Acknowledgements

A. K. K., K. C. P., and L. P. D. gratefully acknowledge financial support under awards R01HL135505 and R21HL139208 from the National Institutes of Health. A. K. K. gratefully acknowledges financial support under award 1751628 from the National Science Foundation. D. L. B. gratefully acknowledges financial support under award 1762705 from the National Science Foundation and award 18CDA34110134 from the American Heart Association.

References

1 J. M. Anderson, A. Rodriguez and D. T. Chang, Presented at *Semin. Immunol.*, 2008, vol. 20, pp. 86.
2 C. M. Jackson and Y. Nemerson, *Annu. Rev. Biochem.*, 1980, **49**, 765.
3 A. P. McGuigan and M. V. Sefton, *Biomaterials*, 2007, **28**, 2547.
4 M. B. Gorbet and M. V. Sefton, *Biomaterials*, 2004, **25**, 5681.
5 M.-C. Sin, Y.-M. Sun and Y. Chang, *ACS Appl. Mater. Interfaces*, 2014, **6**, 861.
6 M. E. Bertrand, V. Legrand, J. Boland, E. Fleck, J. Bonnier, H. Emmanuelson, M. Vrolix, L. Missault, S. Chierchia and M. Casaccia, *Circulation*, 1998, **98**, 1597.
7 M. L. Myers, G. M. Lawrie, E. S. Crawford, J. F. Howell, G. C. Morris Jr, D. H. Glaeser and M. E. Debakey, *J. Am. Coll. Cardiol.*, 1989, **13**, 57.
8 J. L. Moake, N. A. Turner, N. A. Stathopoulos, L. Nolasco and J. D. Hellums, *Blood*, 1988, **71**, 1366.
9 G. Shepherd, P. Mohorn, K. Yacoub and D. W. May, *Ann. Pharmacother.*, 2012, **46**, 169.
10 H. P. Greisler, *Ann. Vasc. Surg.*, 1990, **4**, 98.
11 S. L. Cooper, N. A. Peppas, A. S. Hoffman and B. D. Ratner, *Biomaterials: Interfacial phenomena and applications*, ACS Publications, Washington, DC, USA, 1982.
12 J. H. Lee, B. J. Jeong and H. B. Lee, *J. Biomed. Mater. Res., Part A*, 1997, **34**, 105.
13 R. K. Roy and K. R. Lee, *J. Biomed. Mater. Res., Part B*, 2007, **83**, 72.
14 B. A. Weisenberg and D. L. Mooradian, *J. Biomed. Mater. Res.*, 2002, **60**, 283.
15 M.-C. Sin, S.-H. Chen and Y. Chang, *Polym. J.*, 2014, **46**, 436.
16 S. Braune, C. Sperling, M. Maitz, U. Steinseifer, J. Clauser, B. Hiebl, S. Krajewski, H. Wendel and F. Jung, *Colloids Surf., B*, 2017, **158**, 416.
17 P. H. Lima, S. V. Pereira, R. B. Rabello, E. Rodriguez-Castellón, M. M. Beppu, P. Chevallier, D. Mantovani and R. S. Vieira, *Colloids Surf. B. Biointerfaces*, 2013, **111**, 719.
18 C. S. Campelo, P. Chevallier, J. M. Vaz, R. S. Vieira and D. Mantovani, *Mater. Sci. Eng., C*, 2017, **72**, 682.
19 K. Cai, J. Bossert and K. D. Jandt, *Colloids Surf. B. Biointerfaces*, 2006, **49**, 136.
20 Y. Ding, Y. Leng, N. Huang, P. Yang, X. Lu, X. Ge, F. Ren, K. Wang, L. Lei and X. Guo, *J. Biomed. Mater. Res., Part A*, 2013, **101**, 622.
21 K. R. Milner, A. J. Snyder and C. A. Siedlecki, *J. Biomed. Mater. Res., Part A*, 2006, **76**, 561.
22 P. Roach, D. Farrar and C. C. Perry, *J. Am. Chem. Soc.*, 2006, **128**, 3939.
23 L. B. Koh, I. Rodriguez and S. S. Venkatraman, *Biomaterials*, 2010, **31**, 1533.
24 A. Sethuraman, M. Han, R. S. Kane and G. Belfort, *Langmuir*, 2004, **20**, 7779.
25 W. Song and J. F. Mano, *Soft Matter*, 2013, **9**, 2985.
26 X. Ye, Y.-l. Shao, M. Zhou, J. Li and L. Cai, *Appl. Surf. Sci.*, 2009, **255**, 6686.
27 J. H. Lee and H. B. Lee, *J. Biomed. Mater. Res.*, 1998, **41**, 304.
28 C. Werner, M. F. Maitz and C. Sperling, *J. Mater. Chem.*, 2007, **17**, 3376.
29 Y. Chang, S.-H. Shu, Y.-J. Shih, C.-W. Chu, R.-C. Ruaan and W.-Y. Chen, *Langmuir*, 2009, **26**, 3522.
30 C. Mao, Y. Qiu, H. Sang, H. Mei, A. Zhu, J. Shen and S. Lin, *Adv. Colloid Interface Sci.*, 2004, **110**, 5.
31 A. Solouk, B. G. Cousins, H. Mirzadeh and A. M. Seifalian, *Biotechnol. Appl. Biochem.*, 2011, **58**, 311.
32 J.-H. Jiang, L.-P. Zhu, X.-L. Li, Y.-Y. Xu and B.-K. Zhu, *J. Membr. Sci.*, 2010, **364**, 194.
33 E. Salimi, A. Ghaee, A. F. Ismail, M. H. D. Othman and G. P. Sean, *Macromol. Mater. Eng.*, 2016, **301**, 771.
34 J. A. Davidson, K. P. Daigle and P. Kovacs, *Artif. Organs*, 1996, **20**, 513.
35 P. K. Chu, J. Chen, L. Wang and N. Huang, *Mater. Sci. Eng., R*, 2002, **36**, 143.
36 Y. Qiu, A. C. Brown, D. R. Myers, Y. Sakurai, R. G. Mannino, R. Tran, B. Ahn, E. T. Hardy, M. F. Kee and S. Kumar, *Proc. Natl. Acad. Sci. U. S. A.*, 2014, **111**, 14430.

37 W. C. Chiu, G. Girdhar, M. Xenos, Y. Alemu, J. S. Soares, S. Einav, M. Slepian and D. Bluestein, *J. Biomech. Eng.*, 2014, **136**, 021014.
38 J. R. Gohean, E. R. Larson, B. H. Hsi, M. Kurusz, R. W. Smaling and R. G. Longoria, *ASAIO J.*, 2017, **63**, 198.
39 K. K. Marinescu, N. Uriel and S. Adatya, *Curr. Opin. Cardiol.*, 2016, **31**, 321.
40 P. D. Morris, A. Narracott, H. von Tengg-Kobligk, D. A. S. Soto, S. Hsiao, A. Lungu, P. Evans, N. W. Bressloff, P. V. Lawford, D. R. Hose and J. P. Gunn, *Heart*, 2016, **102**, 18.
41 L. P. Dasi, D. W. Murphy, A. Glezer and A. P. Yoganathan, *J. Biomech.*, 2008, **41**, 1166.
42 D. W. Murphy, L. P. Dasi, J. Vukasinovic, A. Glezer and A. P. Yoganathan, *J. Biomech. Eng.*, 2010, **132**, 071011.
43 J. Puskas, M. Gerdisch, D. Nichols, R. Quinn, C. Anderson, B. Rhenman, L. Fermin, M. McGrath, B. Kong, C. Hughes, G. Sethi, M. Wait, T. Martin and A. Graeve, *J. Thorac. Cardiovasc. Surg.*, 2014, **147**, 1202.
44 M. Liu, Y. Zheng, J. Zhai and L. Jiang, *Acc. Chem. Res.*, 2009, **43**, 368.
45 J. Genzer and K. Efimenko, *Biofouling*, 2006, **22**, 339.
46 B. J. Privett, J. Youn, S. A. Hong, J. Lee, J. Han, J. H. Shin and M. H. Schoenfisch, *Langmuir*, 2011, **27**, 9597.
47 B. Bhushan, Y. C. Jung and K. Koch, *Langmuir*, 2009, **25**, 3240.
48 R. Fürstner, W. Barthlott, C. Neinhuis and P. Walzel, *Langmuir*, 2005, **21**, 956.
49 S. Nishimoto and B. Bhushan, *RSC Adv.*, 2013, **3**, 671.
50 K. M. Wisdom, J. A. Watson, X. Qu, F. Liu, G. S. Watson and C.-H. Chen, *Proc. Natl. Acad. Sci. U. S. A.*, 2013, **110**, 7992.
51 H. Vahabi, W. Wang, S. Movafaghi and A. K. Kota, *ACS Appl. Mater. Interfaces*, 2016, **8**, 21962.
52 S. Vallabhuneni, S. Movafaghi, W. Wang and A. K. Kota, *Macromol. Mater. Eng.*, 2018, **303**, 1800313.
53 B. Bhushan and Y. C. Jung, *Prog. Mater. Sci.*, 2011, **56**, 1.
54 R. J. Daniello, N. E. Waterhouse and J. P. Rothstein, *Phys. Fluids*, 2009, **21**, 085103.
55 J. Ou, B. Perot and J. P. Rothstein, *Phys. Fluids*, 2004, **16**, 4635.
56 S. Pan, A. K. Kota, J. M. Mabry and A. Tuteja, *J. Am. Chem. Soc.*, 2012, **135**, 578.
57 R. Jafari, R. Menini and M. Farzaneh, *Appl. Surf. Sci.*, 2010, **257**, 1540.
58 K. K. Varanasi, T. Deng, J. D. Smith, M. Hsu and N. Bhate, *Appl. Phys. Lett.*, 2010, **97**, 234102.
59 J. B. Boreyko and C. P. Collier, *ACS Nano*, 2013, **7**, 1618.
60 L. Jiang, X. Yao, H. Li, Y. Fu, L. Chen, Q. Meng, W. Hu and L. Jiang, *Adv. Mater.*, 2010, **22**, 376.
61 X. Zhang, J. Zhao, Q. Zhu, N. Chen, M. Zhang and Q. Pan, *ACS Appl. Mater. Interfaces*, 2011, **3**, 2630.
62 T. Liu, S. Chen, S. Cheng, J. Tian, X. Chang and Y. Yin, *Electrochim. Acta*, 2007, **52**, 8003.
63 T. T. Isimjan, T. Wang and S. Rohani, *Chem. Eng. J.*, 2012, **210**, 182.
64 R. Enright, N. Miljkovic, J. L. Alvarado, K. Kim and J. W. Rose, *Nanoscale Microscale Thermophys. Eng.*, 2014, **18**, 223.
65 D. Attinger, C. Frankiewicz, A. R. Betz, T. M. Schutzius, R. Ganguly, A. Das, C.-J. Kim and C. M. Megaridis, *MRS Energy Sustain.*, 2014, **1**, 1.
66 H. Vahabi, W. Wang, S. Davies, J. M. Mabry and A. K. Kota, *ACS Appl. Mater. Interfaces*, 2017, **9**, 29328.
67 N. Miljkovic, R. Enright, Y. Nam, K. Lopez, N. Dou, J. Sack and E. N. Wang, *Nano Lett.*, 2012, **13**, 179.
68 G. Fang, W. Li, X. Wang and G. Qiao, *Langmuir*, 2008, **24**, 11651.
69 Y. Zhao, J. Fang, H. Wang, X. Wang and T. Lin, *Adv. Mater.*, 2010, **22**, 707.
70 S. Movafaghi, W. Wang, A. Metzger, D. Williams, J. Williams and A. Kota, *Lab Chip*, 2016, **16**, 3204.
71 A. Pendurthi, S. Movafaghi, W. Wang, S. Shadman, A. P. Yalin and A. K. Kota, *ACS Appl. Mater. Interfaces*, 2017, **9**, 25656.
72 E. J. Falde, S. T. Yohe, Y. L. Colson and M. W. Grinstaff, *Biomaterials*, 2016, **104**, 87.
73 V. Jokinen, E. Kankuri, S. Hoshian, S. Franssila and R. H. Ras, *Adv. Mater.*, 2018, 1705104.
74 K. Fukagata, N. Kasagi and P. Koumoutsakos, *Phys. Fluids*, 2006, **18**, 051703.
75 T. T. Pham, S. Wiedemeier, S. Maenz, G. Gastrock, U. Settmacher, K. D. Jandt, J. Zanow, C. Lüdecke and J. Bossert, *Colloids Surf. B. Biointerfaces*, 2016, **145**, 502.
76 D. Ding, R. M. Starke, C. R. Durst and A. J. Evans, *Interv. Neuroradiol.*, 2014, **20**, 663.
77 A. Kheradvar, E. M. Groves, C. A. Simmons, B. Griffith, S. H. Alavi, R. Tranquillo, L. P. Dasi, A. Falahatpisheh, K. J. Grande-Allen and C. J. Goergen, *Ann. Biomed. Eng.*, 2015, **43**, 858.
78 G. D. Curfman, S. Morrissey, J. A. Jarcho and J. M. Drazen, *Mass Medical Soc.*, 2007, **356**, 1059.
79 S. H. McKellar, S. Abel, C. L. Camp, R. M. Suri, M. H. Ereth and H. V. Schaff, *J. Thorac. Cardiovasc. Surg.*, 2011, **141**, 1410.
80 B. D. Ratner, *J. Biomed. Mater. Res., Part A*, 1993, **27**, 283.
81 C. N. Jenne and P. Kubes, *Platelets*, 2015, **26**, 286.
82 E. Kolaczkowska and P. Kubes, *Nat. Rev. Immunol.*, 2013, **13**, 159.
83 Y. Yuan, I. Alwis, M. C. Wu, Z. Kaplan, K. Ashworth, D. Bark, A. Pham, J. Mcfadyen, S. M. Schoenwaelder and E. C. Josefsson, *Sci. Transl. Med.*, 2017, **9**, eaam5861.
84 A. Waterhouse, S. G. Wise, M. K. Ng and A. S. Weiss, *Tissue Eng., Part B*, 2011, **17**, 93.
85 D. Labarre, *Trends Biomater. Artif. Organs.*, 2001, **15**, 1.
86 M. V. Sefton, C. H. Gemmell and M. B. Gorbet, *J. Biomater. Sci., Polym. Ed.*, 2000, **11**, 1165.
87 S. Venkatraman, F. Boey and L. L. Lao, *Prog. Polym. Sci.*, 2008, **33**, 853.
88 D. F. Williams, *The Williams dictionary of biomaterials*, Liverpool University Press, Liverpool, UK, 1999.
89 D. J. Brotman, S. R. Deitcher, G. Y. Lip and A. C. Matzdorff, *South. Med. J.*, 2004, **97**, 213.

90 J. F. Viles-Gonzalez, V. Fuster and J. J. Badimon, *Am. Heart J.*, 2005, **149**, S19.
91 T. Watson, E. Shantsila and G. Y. Lip, *Lancet*, 2009, **373**, 155.
92 G. D. Lowe, *Pathophysiol. Haemostasis Thromb.*, 2003, **33**, 455.
93 M. Nobili, J. Sheriff, U. Morbiducci, A. Redaelli and D. Bluestein, *ASAIO J.*, 2008, **54**, 64.
94 J. Jesty, W. Yin, P. Perrotta and D. Bluestein, *Platelets*, 2003, **14**, 143.
95 S. P. Jackson, *Nat. Med.*, 2011, **17**, 1423.
96 Z. M. Ruggeri, *Nat. Med.*, 2002, **8**, 1227.
97 B. Savage, E. Saldívar and Z. M. Ruggeri, *Cell*, 1996, **84**, 289.
98 S. Schneider, S. Nuschele, A. Wixforth, C. Gorzelanny, A. Alexander-Katz, R. Netz and M. Schneider, *Proc. Natl. Acad. Sci. U. S. A.*, 2007, **104**, 7899.
99 M. Bryckaert, J.-P. Rosa, C. V. Denis and P. J. Lenting, *Cell. Mol. Life Sci.*, 2015, **72**, 307.
100 K. A. Jørgensen and E. Stoffersen, *Thromb. Res.*, 1980, **17**, 13.
101 P. Blair and R. Flaumenhaft, *Blood Rev.*, 2009, **23**, 177.
102 J. W. Heemskerk, W. M. Vuist, M. A. Feijge, C. P. Reutelingsperger and T. Lindhout, *Blood*, 1997, **90**, 2615.
103 S. P. Jackson and S. M. Schoenwaelder, *Blood*, 2010, **116**, 2011.
104 S. M. Jobe, K. M. Wilson, L. Leo, A. Raimondi, J. D. Molkentin, S. R. Lentz and J. Di Paola, *Blood*, 2008, **111**, 1257.
105 A. S. Wolberg, *Blood Rev.*, 2007, **21**, 131.
106 A. Onasoga-Jarvis, T. Puls, S. O'brien, L. Kuang, H. Liang and K. Neeves, *J. Thromb. Haemostasis*, 2014, **12**, 373.
107 K. Neeves, D. Illing and S. Diamond, *Biophys. J.*, 2010, **98**, 1344.
108 M. Ghasemzadeh, Z. S. Kaplan, I. Alwis, S. M. Schoenwaelder, K. J. Ashworth, E. Westein, E. Hosseini, H. H. Salem, R. Slattery and S. R. McColl, *Blood*, 2013, **121**, 4555.
109 B. G. Yipp and P. Kubes, *Blood*, 2013, **122**, 2784.
110 T. A. Fuchs, A. Brill, D. Duerschmied, D. Schatzberg, M. Monestier, D. D. Myers, S. K. Wrobleski, T. W. Wakefield, J. H. Hartwig and D. D. Wagner, *Proc. Natl. Acad. Sci. U. S. A.*, 2010, **107**, 15880.
111 K. Martinod and D. D. Wagner, *Blood*, 2014, **123**, 2768.
112 J. M. Anderson, *Cardiovasc. Pathol.*, 1993, **2**, 33.
113 S. Franz, S. Rammelt, D. Scharnweber and J. C. Simon, *Biomaterials*, 2011, **32**, 6692.
114 B. S. Smith, P. Capellato, S. Kelley, M. Gonzalez-Juarrero and K. C. Popat, *Biomater. Sci.*, 2013, **1**, 322.
115 D. M. Higgins, R. J. Basaraba, A. C. Hohnbaum, E. J. Lee, D. W. Grainger and M. Gonzalez-Juarrero, *Am. J. Pathol.*, 2009, **175**, 161.
116 A. Mantovani and E. Dejana, *Immunol. Today*, 1989, **10**, 370.
117 C. Dinarello, *J. Biol. Regul. Homeost. Agents*, 1997, **11**, 91.
118 M. van de Weert, P. I. Haris, W. E. Hennink and D. J. Crommelin, *Anal. Biochem.*, 2001, **297**, 160.
119 H. Yang, G. Luo, P. Karnchanaphanurach, T.-M. Louie, I. Rech, S. Cova, L. Xun and X. S. Xie, *Science*, 2003, **302**, 262.
120 A. A. Khalili and M. R. Ahmad, *Int. J. Mol. Sci.*, 2015, **16**, 18149.
121 S. Kamath, A. Blann and G. Lip, *Eur. Heart J.*, 2001, **22**, 1561.
122 J. G. Kay and S. Grinstein, *Sensors*, 2011, **11**, 1744.
123 M. Noris and G. Remuzzi, *Semin. Nephrol.*, 2013, **33**, 479.
124 U. T. Seyfert, V. Biehl and J. Schenk, *Biomol. Eng.*, 2002, **19**, 91.
125 M. Sanak, B. Jakieła and W. Węgrzyn, *Bull. Pol. Acad. Sci.: Tech. Sci.*, 2010, **58**, 317.
126 F. Jung and S. Braune, *Biointerphases*, 2016, **11**, 029601.
127 W. Anderson, *Int. J. Pet. Technol.*, 1986, **38**, 1.
128 D. Bangham and R. Razouk, *Trans. Faraday Soc.*, 1937, **33**, 1459.
129 X.-M. Li, D. Reinhoudt and M. Crego-Calama, *Chem. Soc. Rev.*, 2007, **36**, 1350.
130 A. K. Kota, G. Kwon and A. Tuteja, *NPG Asia Mater.*, 2014, **6**, e109.
131 R. D. Hazlett, *J. Colloid Interface Sci.*, 1990, **137**, 527.
132 C. Eriksson and H. Nygren, *J. Lab. Clin. Med.*, 2001, **137**, 296.
133 N. Hori, T. Ueno, H. Minamikawa, F. Iwasa, F. Yoshino, K. Kimoto, M. C.-I. Lee and T. Ogawa, *Acta Biomater.*, 2010, **6**, 4175.
134 S. Kidoaki and T. Matsuda, *Langmuir*, 1999, **15**, 7639.
135 K. M. Kovach, J. R. Capadona, A. S. Gupta and J. A. Potkay, *J. Biomed. Mater. Res., Part A*, 2014, **102**, 4195.
136 J. Y. Lim and H. J. Donahue, *Tissue Eng.*, 2007, **13**, 1879.
137 E. Ostuni, R. G. Chapman, R. E. Holmlin, S. Takayama and G. M. Whitesides, *Langmuir*, 2001, **17**, 5605.
138 M. Rixman, D. Dean, C. Macias and C. Ortiz, *Langmuir*, 2003, **19**, 6202.
139 P. Roach, D. Farrar and C. C. Perry, *J. Am. Chem. Soc.*, 2005, **127**, 8168.
140 G. B. Sigal, M. Mrksich and G. M. Whitesides, *J. Am. Chem. Soc.*, 1998, **120**, 3464.
141 Y. Wu, F. I. Simonovsky, B. D. Ratner and T. A. Horbett, *J. Biomed. Mater. Res., Part A*, 2005, **74**, 722.
142 L.-C. Xu and C. A. Siedlecki, *Biomaterials*, 2007, **28**, 3273.
143 A. K. Kota, W. Choi and A. Tuteja, *MRS Bull.*, 2013, **38**, 383.
144 M. Nosonovsky and B. Bhushan, *Curr. Opin. Colloid Interface Sci.*, 2009, **14**, 270.
145 Y. T. Cheng, D. Rodak, C. Wong and C. Hayden, *Nanotechnology*, 2006, **17**, 1359.
146 A. Marmur, *Langmuir*, 2004, **20**, 3517.
147 L. Feng, S. Li, Y. Li, H. Li, L. Zhang, J. Zhai, Y. Song, B. Liu, L. Jiang and D. Zhu, *Adv. Mater.*, 2002, **14**, 1857.
148 H. Vahabi, W. Wang, K. C. Popat, G. Kwon, T. B. Holland and A. K. Kota, *Appl. Phys. Lett.*, 2017, **110**, 251602.
149 W. Wang, K. Lockwood, L. M. Boyd, M. D. Davidson, S. Movafaghi, H. Vahabi, S. R. Khetani and A. K. Kota, *ACS Appl. Mater. Interfaces*, 2016, **8**, 18664.
150 T. Young, *Philos. Trans. R. Soc. London*, 1805, **95**, 65.

151 E. Hare, E. Shafrin and W. Zisman, *J. Phys. Chem.*, 1954, **58**, 236.
152 A. K. Kota, J. M. Mabry and A. Tuteja, *Surf. Innovations*, 2013, **1**, 71.
153 J. Genzer and K. Efimenko, *Science*, 2000, **290**, 2130.
154 T. Nishino, M. Meguro, K. Nakamae, M. Matsushita and Y. Ueda, *Langmuir*, 1999, **15**, 4321.
155 R. N. Wenzel, *Ind. Eng. Chem.*, 1936, **28**, 988.
156 A. Cassie and S. Baxter, *Trans. Faraday Soc.*, 1944, **40**, 546.
157 A. Marmur, *Langmuir*, 2003, **19**, 8343.
158 W. Choi, A. Tuteja, J. M. Mabry, R. E. Cohen and G. H. McKinley, *J. Colloid Interface Sci.*, 2009, **339**, 208.
159 N. A. Patankar, *Langmuir*, 2003, **19**, 1249.
160 L. Gao and T. J. McCarthy, *Langmuir*, 2006, **22**, 2966.
161 R. E. Johnson Jr and R. H. Dettre, *J. Phys. Chem.*, 1964, **68**, 1744.
162 R. H. Dettre and R. E. Johnson Jr, *J. Phys. Chem.*, 1965, **69**, 1507.
163 A. Grigoryev, I. Tokarev, K. G. Kornev, I. Luzinov and S. Minko, *J. Am. Chem. Soc.*, 2012, **134**, 12916.
164 P. Mazumder, Y. Jiang, D. Baker, A. Carrilero, D. Tulli, D. Infante, A. T. Hunt and V. Pruneri, *Nano Lett.*, 2014, **14**, 4677.
165 A. Tuteja, W. Choi, J. M. Mabry, G. H. McKinley and R. E. Cohen, *Proc. Natl. Acad. Sci. U. S. A.*, 2008, **105**, 18200.
166 W. Wang, J. Salazar, H. Vahabi, A. Joshi-Imre, W. E. Voit and A. K. Kota, *Adv. Mater.*, 2017, **29**, 1700295.
167 A. Tuteja, W. Choi, M. Ma, J. M. Mabry, S. A. Mazzella, G. C. Rutledge, G. H. McKinley and R. E. Cohen, *Science*, 2007, **318**, 1618.
168 E. Hrncir and J. Rosina, *Physiol. Res.*, 1996, **46**, 319.
169 D. D. Deligianni, N. Katsala, S. Ladas, D. Sotiropoulou, J. Amedee and Y. Missirlis, *Biomaterials*, 2001, **22**, 1241.
170 J. Ballester-Beltrán, P. Rico, D. Moratal, W. Song, J. F. Mano and M. Salmerón-Sánchez, *Soft Matter*, 2011, **7**, 10803.
171 R. B. Pernites, C. M. Santos, M. Maldonado, R. R. Ponnapati, D. F. Rodrigues and R. C. Advincula, *Chem. Mater.*, 2011, **24**, 870.
172 J. Zhao, L. Song, J. Yin and W. Ming, *Chem. Commun.*, 2013, **49**, 9191.
173 Y. Koc, A. De Mello, G. McHale, M. I. Newton, P. Roach and N. J. Shirtcliffe, *Lab Chip*, 2008, **8**, 582.
174 K. Bartlet, S. Movafaghi, A. Kota and K. C. Popat, *RSC Adv.*, 2017, **7**, 35466.
175 M. Paven, P. Papadopoulos, S. Schöttler, X. Deng, V. Mailänder, D. Vollmer and H.-J. Butt, *Nat. Commun.*, 2013, **4**, 2512.
176 E. S. Leibner, N. Barnthip, W. Chen, C. R. Baumrucker, J. V. Badding, M. Pishko and E. A. Vogler, *Acta Biomater.*, 2009, **5**, 1389.
177 C. Li, W. Ye, J. Jin, X. Xu, J. Liu and J. Yin, *J. Mater. Chem.*, 2015, **3**, 3922.
178 D. L. Bark, H. Vahabi, H. Bui, S. Movafaghi, B. Moore, A. K. Kota, K. Popat and L. P. Dasi, *Ann. Biomed. Eng.*, 2017, **45**, 452.
179 T. Sun, H. Tan, D. Han, Q. Fu and L. Jiang, *Small*, 2005, **1**, 959.
180 C. Mao, C. Liang, W. Luo, J. Bao, J. Shen, X. Hou and W. Zhao, *J. Mater. Chem.*, 2009, **19**, 9025.
181 S. Hoshian, E. Kankuri, R. H. Ras, S. Franssila and V. Jokinen, *Sci. Rep.*, 2017, **7**, 16019.
182 M. Khorasani and H. Mirzadeh, *J. Appl. Polym. Sci.*, 2004, **91**, 2042.
183 M. Zhou, J. H. Yang, X. Ye, A. R. Zheng, G. Li, P. F. Yang, Y. Zhu and L. Cai, *J. Nano Res.*, 2008, **2**, 129.
184 S. Moradi, N. Hadjesfandiari, S. F. Toosi, J. N. Kizhakkedathu and S. G. Hatzikiriakos, *ACS Appl. Mater. Interfaces*, 2016, **8**, 17631.
185 S. Movafaghi, V. Leszczak, W. Wang, J. A. Sorkin, L. P. Dasi, K. C. Popat and A. K. Kota, *Adv. Healthcare Mater.*, 2017, **6**, 1600717.
186 C. Q. Lai, J. C. W. Shen, W. C. W. Cheng and C. H. Yap, *RSC Adv.*, 2016, **6**, 62451.
187 D. L. Bark, A. N. Para and D. N. Ku, *Biotechnol. Bioeng.*, 2012, **109**, 2642.
188 D. L. Bark Jr and D. N. Ku, *Biophys. J.*, 2013, **105**, 502.
189 S. Einav and D. Bluestein, *Ann. N. Y. Acad. Sci.*, 2004, **1015**, 351.
190 W. S. Nesbitt, E. Westein, F. J. Tovar-Lopez, E. Tolouei, A. Mitchell, J. Fu, J. Carberry, A. Fouras and S. P. Jackson, *Nat. Med.*, 2009, **15**, 665.
191 A. L. Fogelson and K. B. Neeves, *Annu. Rev. Fluid Mech.*, 2015, **47**, 377.
192 P. R. Jones, X. Hao, E. R. Cruz-Chu, K. Rykaczewski, K. Nandy, T. M. Schutzius, K. K. Varanasi, C. M. Megaridis, J. H. Walther, P. Koumoutsakos, H. D. Espinosa and N. A. Patankar, *Sci. Rep.*, 2015, **5**, 12311.
193 M. Xu, G. Sun and C.-J. Kim, *Phys. Rev. Lett.*, 2014, **113**, 136103.
194 N. A. Patankar, *Langmuir*, 2016, **32**, 7023.
195 N. Cohen, A. Dotan, H. Dodiuk and S. Kenig, *Mater. Manuf. Processes*, 2016, **31**, 1143.
196 K. Golovin, M. Boban, J. M. Mabry and A. Tuteja, *ACS Appl. Mater. Interfaces*, 2017, **9**, 11212.
197 T. Verho, C. Bower, P. Andrew, S. Franssila, O. Ikkala and R. H. Ras, *Adv. Mater.*, 2011, **23**, 673.
198 Y. C. Jung and B. Bhushan, *ACS Nano*, 2009, **3**, 4155.
199 Y. Xiu, Y. Liu, D. W. Hess and C. Wong, *Nanotechnology*, 2010, **21**, 155705.